Design and analysis of the main passive RF components for the DTT ICRH system

Francesco Mirizzi [1]*, *Gian Luca* Ravera[2], *Silvio* Ceccuzzi[3], *Sandra* Greco[2], and *Angelo A.* Tuccillo[1]

[1]CREATE Consortium, 80125 Napoli, Italy
[2]ENEA CR Frascati, 00044 Frascati (Rome), Italy
[3]DTT S.C.ar.l., 00044 Frascati (Rome), Italy

Abstract. The Divertor Tokamak Test (DTT) is a new facility designed by Italian DTT Limited Liability Consortium (S.C.ar.l.) [1] aimed at validating an integrated solution for the power exhaust in support of DEMO [2]. The ICRH system, part of the DTT complex of additional heating systems, in its final configuration shall couple to the plasma up to 6 MW in the 60–90 MHz frequency range. All the main radiofrequency passive components of the system have been designed and optimized with the Ansys High Frequency Structures Simulator (HFSS) computer code. In particular 3 dB hybrid couplers, stubs, stretchers and vacuum feedthroughs have been examined. Results of the optimization of these components are presented and discussed in this paper.

1 ICRH system layout

The ICRH system for DTT is conceived in modular units [3]. Each module (Fig. 1) is powered by four, high power, high frequency, solid state generators (SSPG). Each SSPG has an output nominal power of 1.2 MW.

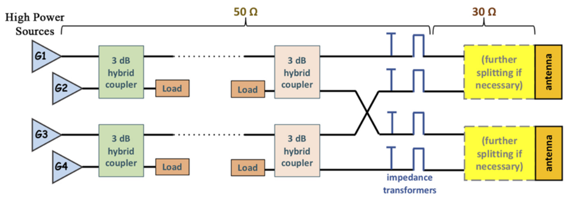

Fig. 1. DTT ICRH system: simplified block schematic.

The power of each module is coupled to the plasma by two independent, three double folded, current straps launchers, which HFSS model is shown, without Faraday screen, in Fig. 2.

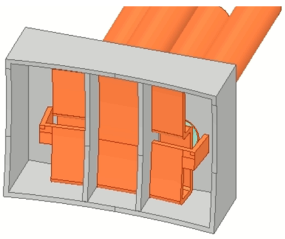

Fig. 2. The three straps ICRH launcher.

In Fig. 1 the power generated by two SSPGs is conveyed, by means of a 3dB *hybrid coupler, rated for a power of 2.5 MW, in a single 50 Ω, 9 and 3/8 inches, coaxial cable: the Main Transmission Line (MTL). Close to the launcher this power is split again, by means of a second 3dB hybrid coupler, in two independent cables, the Local Transmission Lines (LTL), for adequately feed in parallel the six straps of two launchers, with a 0–π–0 phase configuration between the three straps of each launcher [3]. Then impedance matching units, based on stubs and stretchers, transfer the RF power to 30 Ω coaxial cables. All these cables, from the SSPGs to the launchers, are pressurized with dry air at 2 Barg to reduce the risk of possible internal electrical discharges. The launcher instead is at the very low pressure of the DTT vacuum vessel. Therefore, vacuum feedthroughs, with ceramic windows, separate the LTLs from the coaxial cables directly connected to the launcher.

2 General condition of simulation

In this preliminary analysis the central conductor of the coaxial cables is considered in copper and the dielectric layer air. The external shields of the coaxial cables have not been drawn because in HFSS all the model surfaces exposed to the background are considered Perfect Electric Conductor (PEC). During the present analysis, the possibility arose of using components and coaxial cables decommissioned from JET, which characteristic impedance is 30 Ohm. Consequently, the analysis already performed were adapted to a characteristic impedance of 30 Ohms. All the input/output coaxial cables hence have a characteristic impedance $Z_0 = 30\ \Omega$. Their central conductors have a radius of 46 mm and consequently the inner radius of the shields is 75.9 mm. All the HFSS models of the examined components are

* Corresponding author: francesco.mirizzi@outlook.it

fully parameterized so that components with different characteristic impedance, if requested, can be easily modelled and analysed. The optimizations of all the examined components have been performed at 75 MHz, the average frequency of the envisaged operational frequency band, and all the graphs have been obtained in the frequency range 50 – 100 MHz.

3 The single section 3dB hybrid coupler

For this component, due to the high RF power level to be handled (2.5 MW), it has been chosen the branch–line configuration [4], a configuration used in others existing ICRH systems. The HFSS model of a single section branch–line coupler is given in Fig. 3.

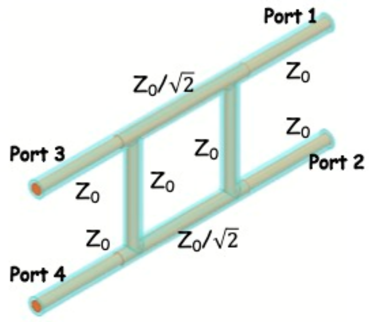

Fig. 3. Single section 3dB branch line coupler.

The theoretical impedances of all the branches of the coupler, each one with a geometrical lengths λ/4, are given in the figure. The optimization has been performed by leaving unchanged the inner radius of the coaxial shield, by changing the radius of the inner conductors of the two horizontal central branches, for obtaining their requested characteristic impedances, and the lengths of all the four central branches, thus preserving the square shape of the section. The optimized sizes of this coupler are shown in Table 1.

Table 1. Single section coupler optimized sizes.

Input/output coaxial length	1000 mm
30 Ω coaxial inner conductor radius	46 mm
30 Ω coaxial shield inner radius	75.9 mm
21 Ω coaxial inner conductor radius	53,8 mm
Vertical branches height	1062 mm

In Fig. 4 is given the amplitude of the reflection coefficients at port 1 (S_{11}) and the amplitudes of the coupling coefficients between ports 1 and 3 (S_{13}) and between ports 1 and 4 (S_{14}) as function of frequency.

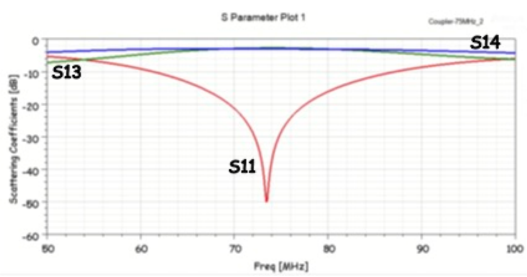

Fig. 4. Single section coupler. S–coefficients amplitude.

The coupler model is symmetric with reference to its input and output ports, so that the reflection coefficients for all the four ports are equal to S_{11} while the coupling coefficient S_{24} is equal to S_{13}, as far as S_{23} is equal to S_{14}. The amplitude of S_{11} is lower than –30 dB in the frequency range 72.2 – 74.7 MHz. A maximum decoupling of 0.3 dB between S_{13} and S_{14} is obtained in the frequency range 67 – 83.3 MHz. If this decoupling is considered acceptable, this component could be effectively used in this band. If not, a better optimization could be performed, but a reduction of the maximum decoupling around the optimization frequency of 75 MHz will result in a significant reduction of the above frequency band. The phase shifts between S_{13} and S_{14} as function of frequency is given in Fig. 5.

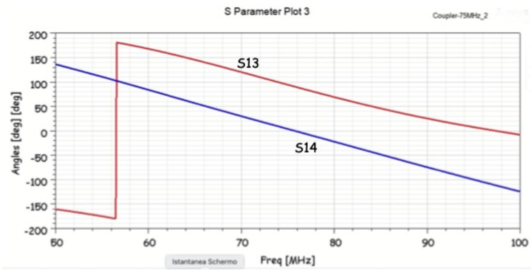

Fig. 5. Single section coupler. S–coefficients phases.

This phase shift is 90±1 degree in the frequency range 66 – 80 MHz, with a satisfactory value of 90.2 degree at 75 MHz.

3.1 The double section 3dB hybrid coupler

A double section branch–line coupler (Fig. 6) has been also analysed for verifying its RF performance.

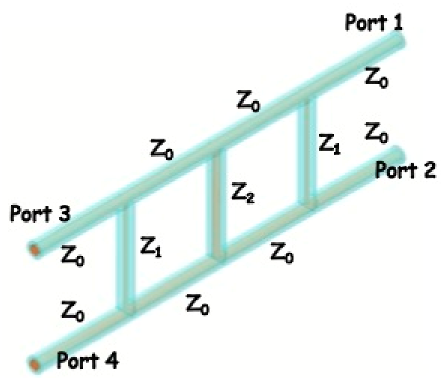

Fig. 6. Double section branch–line coupler.

If Z_0 is the characteristic impedance of the input/output coaxial cables, then the theoretical values of the characteristic impedance of the three vertical branches are:

$$Z_1 = \left(1 + \sqrt{2}\right) \cdot Z_0 \,,$$

$$Z_2 = \sqrt{2} \cdot Z_0 \,,$$

and the theoretical length of the seven central branches (vertical and horizontal) forming the two squares, is λ/4. For the optimization the inner radius of the coaxial shield has been left unchanged for all the branches, as well as the radius of the whole upper and lower horizontal central conductors. The optimization has been performed by varying the radii and the lengths of the three central vertical conductors and the lengths of the four horizontal conductors forming the two squares.

Table 2. Double sections coupler optimized sizes.

Input/output coax length	1000 mm
30 Ω coaxial inner conductor radius	46 mm
Side vertical conductors radius	19 mm
Central vertical conductor radius	36.5 mm
Vertical conductors' height	1000 mm
Centre horizontal conductors' length	1000 mm

The optimized sizes of the main components of the coupler are given in Table 2. In Fig. 7 are given the amplitude of the reflection coefficient at port 1 (S_{11}) and the amplitudes of the coupling coefficients S_{13} and S_{14} as function of frequency.

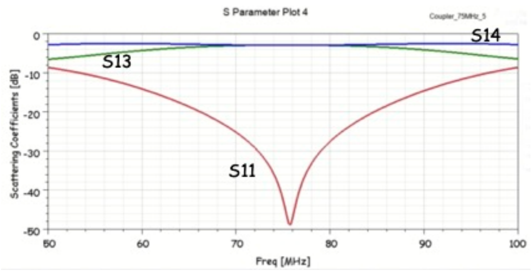

Fig. 7. Double section coupler. S–coefficients amplitude.

Also in this case the amplitude of the reflection coefficients for all the four ports are equal to S_{11} and the amplitude of the coupling coefficient S_{24} is equal to S_{13}, as well as S_{23} is equal to S_{14}. The amplitude of S_{11} is lower than –30 dB in the frequency range 72.4 – 78.8 MHz. A maximum decoupling of 0.3 dB between S_{13} and S_{14} is obtained in the frequency range 68.6 – 82.4 MHz. The phase shift between S_{13} and S_{14} as function of frequency is given in Fig. 8. This phase shift is 90±1 degree in the frequency range 66–89 MHz.

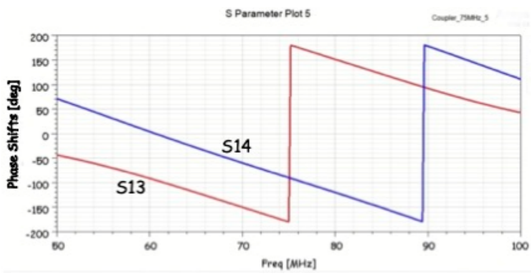

Fig. 8. Double section coupler. S–coefficients phases.

All these values are not significantly different from those obtained for the single-section coupler. Therefore, the relatively greater complexity of the construction of a two-section coupler does not justify its use in the ICRH system for DTT.

4 The stretcher

The stretcher (Fig. 9), also called phase shifter or trombone, is a very simple unit; it determines the lengthening of a transmission line (TL) introducing, at the same time, an additional phase shift respect to a reference TL It is not necessary to use a simulation to optimise this component, as it is sufficient to determine the difference in length between the reference straight line TL, L_{Ref}, and the stretcher.

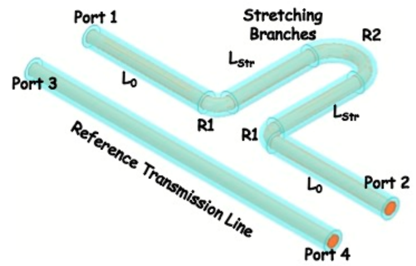

Fig. 9. The stretcher unit.

If L_0 is the length of both the input and output coaxial cables of the stretcher, R_1 the radius of its two lower bends, R_2 that of its upper bend and L_{Str} the length of each one of the two extendable arms of the stretcher, then its overall length:

$$L_{Sh} = 2 \times \left(L_0 + \frac{\pi \cdot R_1}{2} + L_{Str}\right) + \pi \cdot R_2 \ .$$

The corresponding length of the reference straight coaxial cable is:

$$L_{ref} = 2 \cdot L_0 + 2 \cdot (R_1 + R_2) \ .$$

Therefore, the length difference between the reference coaxial cable and the stretcher is:

$$\Delta L = 2 \cdot L_{Str} + (\pi - 2) \cdot (R_1 + R_2)$$

and the phase shift introduced by the stretcher is:

$$\Delta\varphi = \frac{2\pi}{\lambda} \cdot \Delta L \ ,$$

only depending on the length L_{Str} of the two stretching branches and on the operational frequency of the unit through the wavelength λ. Therefore, once defined the phase shift to be introduced by the stretcher, it will be sufficient to adjust the length of its two stretching branches.

5 The stub

The stub, in association with the stretcher, provides to the matching between the 30 Ω transmission line and the connected strap impedance. Three types of stub units have been analysed: a single stub unit, a double stub unit and a triple stub one.

5.1 The single stub matching unit

The stub is a transmission line (TL) connected in parallel to the MTL and closed in short circuit on its free termination (Fig. 10).

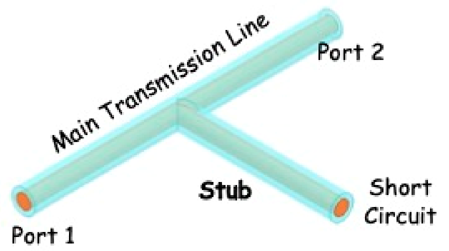

Fig. 10. The single stub matching unit.

The stub impedance is:

$$Z_{St} = Z_0 \cdot \tan \beta L \,,$$

where Z_0 is the characteristic impedance of the stub coaxial cable, $\beta = 2\pi/\lambda$ the phase constant of this cable and L is the stub length. By varying the stub length, the impedance of an unmatched load connected to port 2 is conveniently matched to port 1, that is to the MTL impedance. The optimized dimensions of this stub are shown in Table 3.

Table 3. Single stub unit optimized sizes.

MTL length	2000 mm
Central Conductor radius	46 mm
Coaxial Shield inner radius	75.9 mm
Stub length	1070 mm

Its scattering coefficients as function of frequency are shown in Fig. 11.

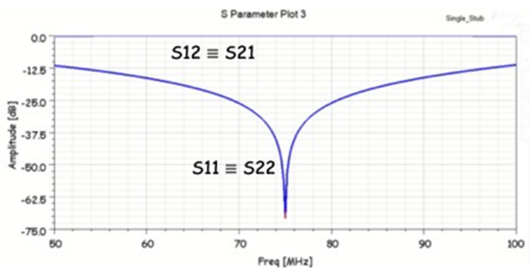

Fig. 11. Single stub unit. S–coefficients amplitude.

The coupling coefficients S_{12} and S_{21} are greater than -0.1 dB in the 60 – 90 MHz frequency band so that their curves are not visible in Fig. 11. Considering the reflection coefficients S_{11} and S_{22} (- 74 dB at 75 MHz and less than -37.5 dB in the 74 – 76 MHz band) this stub should be considered a narrow band component.

5.2 The double stub matching unit

The RF performance of a double stub matching unit (Fig. 12) have been then analysed. The lengths of the two stubs, during this preliminary analysis, have been kept strictly equal to each other. In real operations, instead, the length of each individual stub will be independently adjusted according to the working frequency for obtaining the best impedance matching,

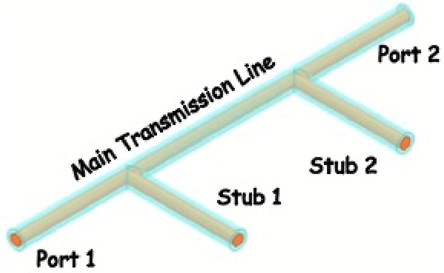

Fig. 12. The double stub matching unit.

The theoretical distance between their axes is initially set to 3λ/8. The optimized sizes of this stub unit are given in Table 4.

Table 4. Double stub unit optimized sizes.

Input/Output Coaxial Length	1000 mm
Central Conductor radius	46 mm
Coaxial shield inner radius	75.9 mm
Centre Conductor Length	1500 mm
Stubs Length	900 mm

Its scattering coefficients as function of frequency are shown in Fig. 13. The coupling coefficients S_{12} and S_{21} are greater than -0.1 dB in the 54.4 – 99.4 MHz frequency range. The reflection coefficients S_{11} and S_{22} in the same frequency range are lower than -16.5 dB, and present two peaks at 59 MHz (-66 dB) and at 90 MHz (-66 dB).

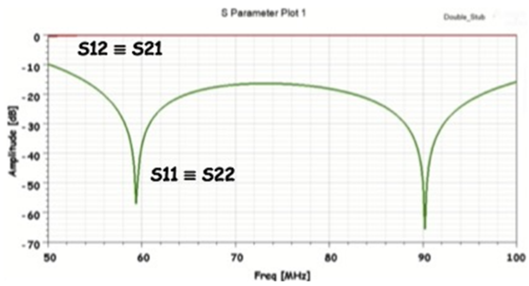

Fig. 13. Double stub unit. S–coefficients amplitude

5.3 The triple stub matching unit

To complete the analysis a triple stub matching unit (Fig. 14) has been examined. The theoretical distance between adjacent stub axes has been initially set to λ/8. The lengths of the three stubs, during this preliminary analysis, have been kept strictly equal to each other, but will be independently adjusted in the real operations.

The optimized sizes of this unit are reported in Table 5.

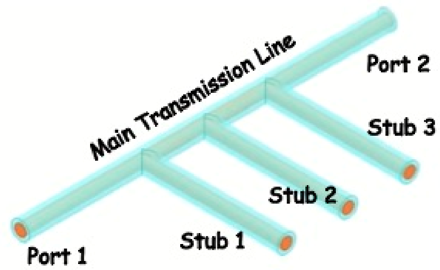

Fig. 14. The triple stub matching unit.

Table 5. Triple stub unit optimized sizes

Input/Output coaxial length	1000 mm
Central conductor radius	46 mm
Coaxial shield inner radius	75.9 mm
Centre conductors' length	508 mm
Stubs length	1185 mm

The scattering coefficients are reported in the following Fig 15. The transmission coefficients S_{12} and S_{21} are greater than -0.12 dB in the 60 – 90 MHz frequency band. The reflection coefficients are lower than -25 dB in the 67.8 – 90 MHz frequency range and present two peaks at 68 MHz (-50 dB) and at 82 MHz (-58 dB).

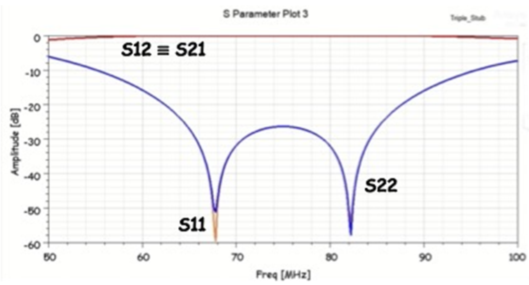

Fig. 15. Triple stub unit. S–coefficients amplitude.

In conclusion these last two analysed stub units should be considered narrow band components and their major realization and operational complexities do not justify their choice for the DTT ICRH system. Anyhow it must be verified if, by changing independently the lengths of their two or three stubs, there will be some significantly improvement in their RF performance.

6 The vacuum feedthrough

Feedthroughs based on ceramic windows [4] are used to separate the pressurized sections of the transmission lines, connected to the high-power RF generator, from their high vacuum section connected to the launcher. The feedthrough's window must withstand the pressure gradient between its two faces and, at the same time, must be shaped for reducing the risk of electric discharge on its surfaces. Feedthroughs with two ceramic windows are commonly used in ICRH systems; the pressure in the space between the two windows is constantly monitored to protect the vacuum vessel from the breaking of any of the two windows. A feedthrough with conic windows has been analysed and compared to a feedthrough with ceramic corrugated disk windows.

6.1 Feedthrough with conic windows

Feedthrough with conic windows have been used on several machines including JET. In Fig. 16 it is reported the HFSS model of a feedthrough with a double conic window [5, 6] that has been analysed taking into account the simulation conditions exposed in the section 2 of this paper.

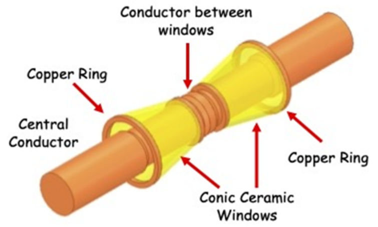

Fig. 16. Feedthrough with a double conic window.

The thickness of the windows has been set to 10mm. The copper rings, used for brazing the windows to the central conductor and to the coaxial cable shield, have a thickness of 10 mm. In Fig. 16 the dielectric is not shown for putting in evidence the feedthrough structure. To maintain constant the characteristic impedance of the device, the dielectric outer radius has been left unchanged while the central conductor radius has been changed in the areas covered by the windows taking into account the dielectric constant of the ceramic (Al_2O_3, $\varepsilon_r = 9.8$). The optimisation, having as targets the minimization of the reflection coefficients at both the ports and the maximization of the transmission coefficients between the ports, has considered the length of the conic windows, their distance, the diameter of the conductor between the two windows and the diameter of the conductor in the areas covered by the two windows. Conductors with different diameters have been connected with conical fittings which length has been optimized too. The optimized dimensions of this component are given in Table 6.

Table 6. Feedthrough with conic windows optimized sizes.

Conductor in the windows area radius	40 mm
Conductor in the windows area length	153 mm
Windows length	133 mm
Conical fittings length	10 mm
Conductor between windows length	18mm
Conductor between windows radius	45 mm

The reflection coefficients as function of the frequency are given in the following Fig. 17 and result lower than -63 dB all over the 60 – 90 MHz frequency band.

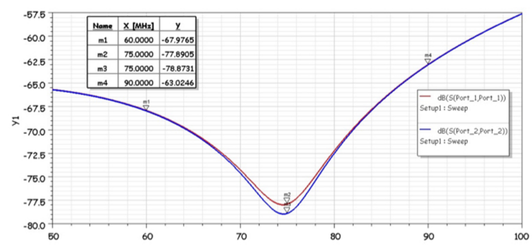

Fig. 17. Feedthrough with conic windows. Reflection coefficients.

The transmission coefficient S_{12} and S_{21} are higher than -1.1×10^{-3} dB in the same frequency range. Therefore, this feedthrough could be profitably used in the DTT ICRH system. The electric field amplitude in this feedthrough, for an input power of 1 MW, is shown in Fig. 18.

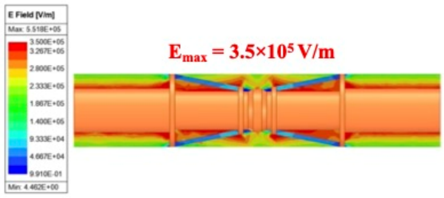

Fig. 18. Electric field amplitude in the feedthrough.

According to this figure, maximum E–field values of about 3.5×10^5 V/m are generated in the reduced volumes between the windows and the central conductor, even under conditions of good matching. In case of strong power reflection from the plasma, these E-fields could be increased up to values able to generate destructive electric breakdowns in those regions. These E–fields are normal to the surface of the central conductor. The component parallel to the surface of the window, in their turn, could generate electric discharges along these surfaces. Therefore, the use of these windows mut be carefully evaluated.

6.2 Feedthrough with corrugated disk windows

Feedthroughs with flat ceramic disk windows are commercially available, but they could undergo potentially destructive electrical arching along their surfaces when used at relatively high RF power, i.e., when in presence of high RF power reflections. To increase the path of possible electrical discharges along their two exposed surfaces, these surfaces can be suitably corrugated [5,6]. A cosine corrugation (Fig. 19.a) has been analysed for the windows of a proposed feedthrough for the DTT ICRH system. The corrugation has been designed for having the maximum cosine amplitudes in correspondence of the central conductor and of the shield of the coaxial cable, where the window should be brazed. The effective path length for a surface electrical arching depends both on the cosine amplitude and on the number of corrugations. A feedthrough with a double corrugated disk window (Fig. 19.b) has been optimised by varying the cosine amplitude, the distance of the two windows and the radius of the conductor between them.

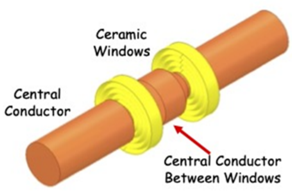

Fig. 19.a. The ceramic corrugated disk window

Fig. 19.b. FT with double corrugated ceramic disk

Also for this model the coaxial dielectric is not shown. The characteristic impedance of the device has been kept constant by leaving unchanged the outer radius of the dielectric while the central conductor radius has been changed in the windows areas according to the dielectric constant of the ceramic. Conductors with different radii have been connected with conical fittings which length has been optimized too. The optimized dimensions are given in Table 7.

Table 7. Feedthrough with corrugated disk windows: optimized sizes.

Window minimum thickness	10 mm
Window central hole radius	28 mm
Cosine amplitude	5 mm
Cosine period	11.975 mm
Number of periods	4
Conductor between windows length	54.6 mm
Conductor between windows radius	49.8 mm

The transmission coefficients of this unit are greater than -7.5 × 10^{-4} dB on the whole operational frequency band of the ICRH system. Its reflection coefficients S_{11} and S_{22}, shown in Fig. 20, results lower than -77 dB on the same frequency range. According to these values, this component presents better performance of the previous analysed feedthrough with conic windows.

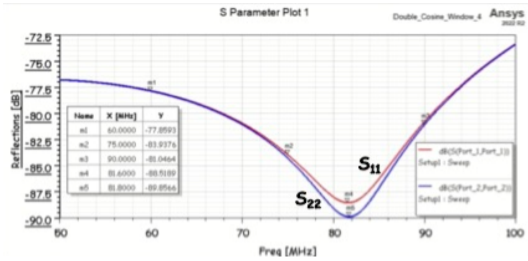

Fig. 20. Feedthrough with corrugated disk windows, reflection coefficients.

The electric field amplitude in this feedthrough, determined by an input RF power of 1 MW, is shown in Fig. 21.

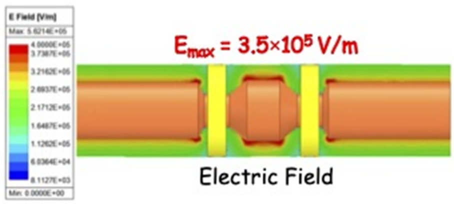

Fig. 21. E–field amplitude in the feedthrough.

Unlike the previous one, in this feedthrough there are no concentration of high electric fields in narrow volumes, hence it should be more resilient to electric discharges. Taking into account the values of the scattering parameters, this component may be more suitable for the ICRH system for DTT.

7 Conclusions

A preliminary analysis of the main RF components of the transmission line of the ICRH system for DTT has been performed with the HFSS code and some indication on their possible use on this system have been given. A more detailed analysis, taking into account other considerations should be carried out before arriving at the final choice.

This work has been carried out in the frame of DTT activities. The authors are very grateful to all the DTT S.C.ar.l. colleagues for their precious contribution.

References

1. F. Romanelli et al., Divertor Tokamak Test Facility project: status of design and implementation, Nucl. Fusion **64**, 112015 (2024). https://doi.org/10.1088/1741-4326/ad5740
2. A. Cardinali et al., Study of ion cyclotron heating scenario and fast particle generation in the Divertor Tokamak Test (DTT) facility, Plasma Physics and Controlled Fusion **62**, 044001 (2020). https://doi.org/10.1088/1361-6587/ab73da
3. S. Ceccuzzi et al., Conceptual definition of an ICRF system for the Italian DTT, Fus. Eng. Des **146**, 361364 (2019). https://doi.org/10.1016/j.fusengdes.2018.12.068
4. Wong Fai-leung, A novel branch-line coupler design for dual band applications, Master thesis, The Chinese University of Hong Kong, July 2004.
5. Ts. Fujii, S. Moriyama: High-Voltage Test of Feedthroughs for a High-Power ICRF Antenna, IEEE Trans. on Plasma Science **29**, 318 (2001). https://doi.org/10.1109/27.922741
6. F. Mirizzi et al., Comparative analysis of vacuum feedthroughs for the DTT ICRH system, IEEE Trans. On Plasma Science **52**, 3710 (2024). https://dx.doi.org/10.1109/tps.2024.3439270
7. S. Greco et al., RF modelling and design of feedthroughs for the ICH system of DTT, Fus. Eng. Des **216**, 115101 (2025). https://doi.org/10.1016/j.fusengdes.2025.115101